Electronic Supplementary Material (ESI) for Journal of Materials Chemistry A.

Supplementary Information

High-yield synthesis of single-crystal silicon nanoparticles as anode materials of lithium ion batteries via photosensitizer-assisted laser pyrolysis

Seongbeom Kim, Chihyun Hwang, Song Yi Park, Seo-Jin Ko, Hyungmin Park, Won Chul Choi, Jong Bok Kim, Dong Suk Kim, Soojin Park, Jin Young Kim* and Hyun-Kon Song*

An optical configuration

To protect from thermal expansion of a ZnSe window installed in the reactor, a raw laser beam (beam diameter 4 mm, defined by $1/e^2$ intensity) is expanded two fold using a beam expander. An expanded laser beam is focused using a ZnSe plano-convex lens into the reactor chamber. The waist of a beam (w_0) at the focusing point is calculated to be 0.43 mm considering terms of diffraction and aberration.

$$w_0 = \frac{4\lambda M^2 f}{\pi D} + k\frac{D^3}{f^2} = 0.43(mm)$$

λ (laser wavelength) : 0.0106 mm,
M^2 (laser beam divergence): 1.3,
f (focal length) : 150 mm,
D (expanded beam aperture) : 8 mm
k (index of refraction function, plano-convex) : 0.0286

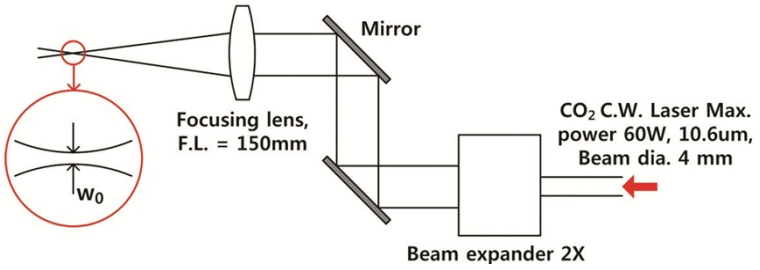

Fig. S1 An optical configuration of the laser pyrolysis set-up.

Dimensions of gas supply tubes and a laser beam

An inner gas supply tube is designed to a semi-elliptical shape rather than a circular type to increase overlap area between reactant gas flow and a laser beam path. A focused laser beam is aligned to locate at the inner tube position where the reactant gas flow, and the beam waist can be assumed to be uniform within inner tube region according to Gaussian beam propagation equation. Z-axis stands for the beam path direction.

$$w(z)^2 = w_0^2(1 + az^2) \text{ , with } w(f)^2 = w_0^2(1 + af^2) = D^2, \quad \therefore a = \frac{1}{f^2}\left(\frac{D^2}{w_0^2} - 1\right)$$

$$\therefore w(z) = w_0\sqrt{(1 + az^2)} = w_0\sqrt{\left(1 + \frac{1}{f^2}\left(\frac{D^2}{w_0^2} - 1\right)z^2\right)}$$

$$= 0.43\sqrt{\left(1 + \frac{1}{150^2}\left(\frac{8^2}{0.43^2} - 1\right)z^2\right)}$$

Then, the beam waist at the end of inner tube can be estimated,

$at\ z = 1\ mm,$

$$w(1) = 0.43\sqrt{\left(1 + \frac{1}{150^2}\left(\frac{8^2}{0.43^2} - 1\right)1^2\right)} = 0.43$$

It implies that the depth of focus in this optical configuration is large enough comparing with a dimension of a gas supply tube. Therefore gas supply tubes and laser beam can be described as Fig. S2.

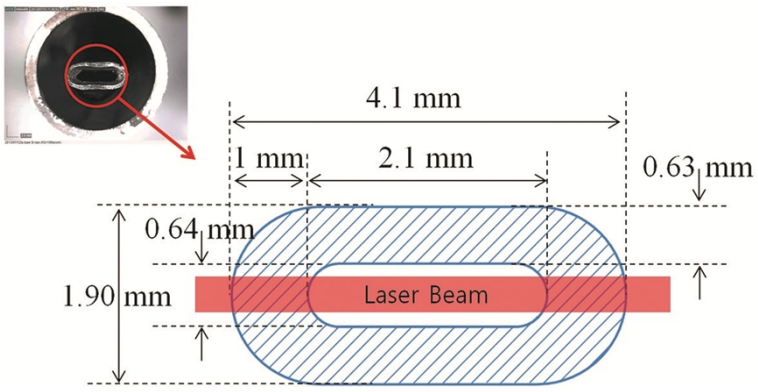

Fig. S2 Dimensions of gas supply tubes and a laser beam path.

Computation fluid dynamics analysis of the gas flows

To estimate the gas flows which undergo interaction with a laser beam, a numerical approach has been done. 368,064 elements were generated based on the model which is very close to physical dimensions of the real reactor as shown in Fig. S3.

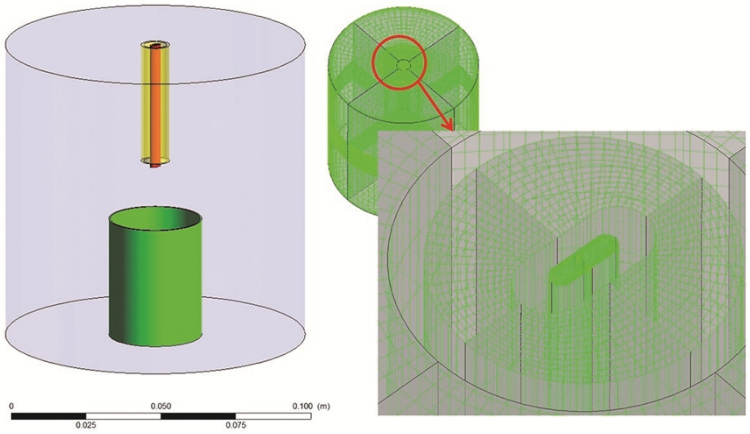

Fig. S3 A geometry of a model and its grids.

Ideal gas and isothermal process (T=25°C) were assumed and experimental gas flow rates and pressure condition were applied for the calculation. Reynolds numbers was blow than 100, therefore, it is considered as a laminar flow problem. Calculation results show that SiH_4 gas in the inner tube is jetted from the end of the tube straight forward to the tube connected to a vacuum pump without being mixed with helium gas as shown in Fig. S4.

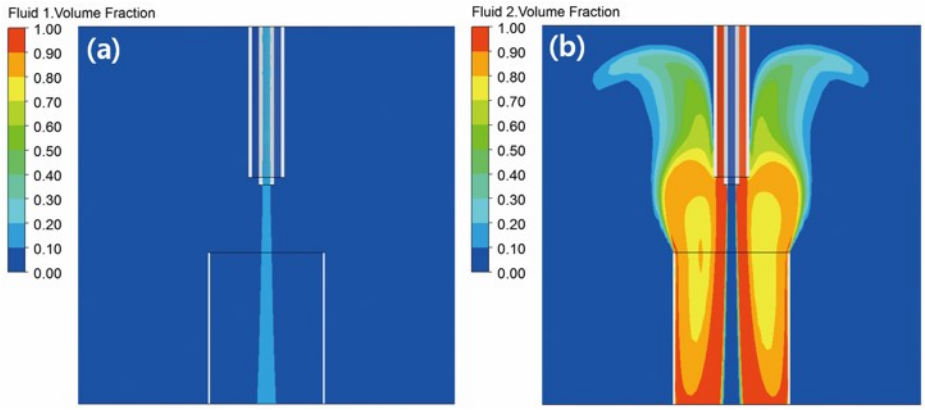

Fig. S4 The gas flow volume fraction maps of SiH_4 (a) and He (b).

Fig. S5 shows cross sectional distribution of SiH_4 flow inside the inner tube and after jetting from the tube. Most of SiH_4 gas flows through the center of the tube, because of the friction against the tube wall. In the reaction zone, below the 2 mm from the tip of the inner tube, only 61.3 % of SiH_4 molecules pass through the laser beam path. Because the laser beam does not cover total area of the inner tube and the diffusion of SiH_4 after jetting is unavoidable.

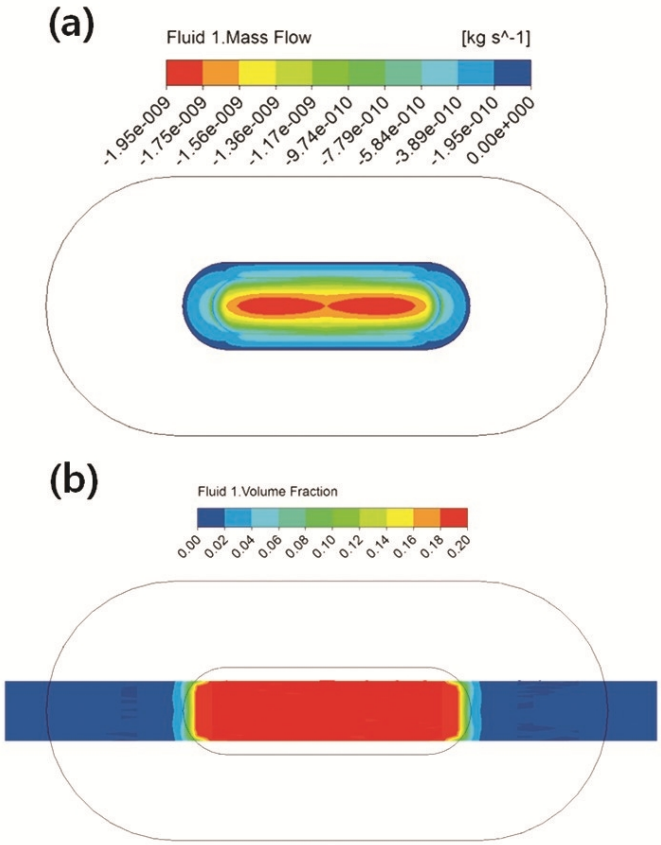

Fig. S5 (a) Distribution of SiH_4 mass flow inside the inner tube. (b) Distribution of SiH_4 volume fraction at the laser beam plane. A distribution map is displayed only in a laser beam path region, colored long rectangular region. The laser beam path is located 2 mm down from the tip of the inner gas tube, crossing the center of gas stream line. Calculated SiH_4 mass flow fraction within the laser beam path is 61.3 %.

Gas-to-solid conversion ratio

The gas-to-solid conversion ratio is calculated after measuring the mass of collected Si-NPs. The equation includes total mass of SiH_4 gas, a mass fraction term of SiH_4 gas which passes through the laser beam path and molar mass ratio of silicon to SiH_4, since H_2 gas is by-products as a result of SiH_4 dissociation process.

$$m_{si} = \eta \cdot k \cdot \dot{m}_{SiH_4} \cdot t \cdot \frac{M_{Si}}{M_{SiH_4}}$$

m_{si} : mass of Si-NPs
η : gas-to-solid conversion ratio
k : mass fraction of SiH_4 which pass through the laser beam path. ~ 0.613
$\dot{m}_{SiH4}$: mass flow rate of SiH_4
t : synthesis time
M_{Si} : silicon molar mass
M_{SiH4} : SiH_4 molar mass

Table S1 The gas-to-solid conversion ratio depending on the gas flow conditions.

SiH_4 gas flow rate (sccm)	H_2 gas flow rate (sccm)	SF_6 gas flow rate (sccm)	Gas-to-solid conversion ratio (%)
25	0	0	12.4
		5	75.0
		10	-
	100	0	7.8
		5	52.4
		10	97.1
		15	16.3

Fig. S6 A video clip of the detonation process. (Referring to a separate video clip file or http://www.youtube.com/watch?v=Ci5z62L8LmE)

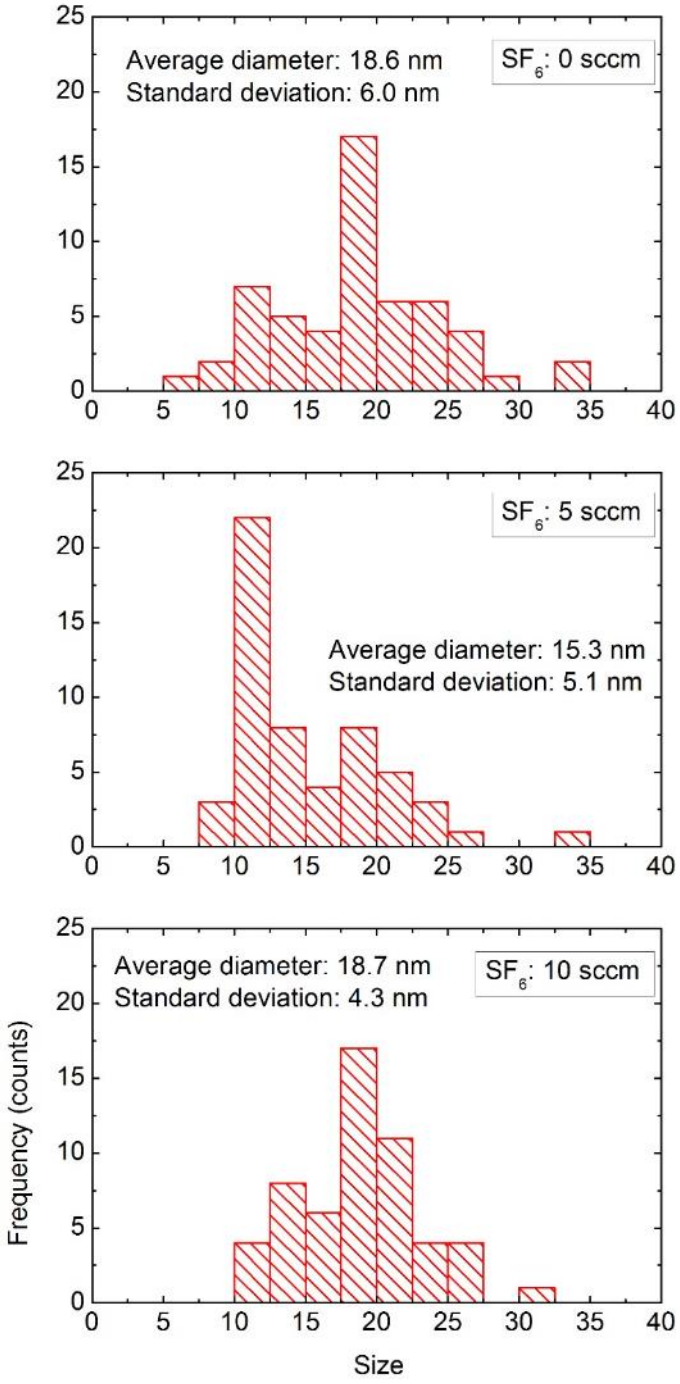

Fig. S7 Size distributions of Si-NPs counting more than 50 NPs from TEM images.

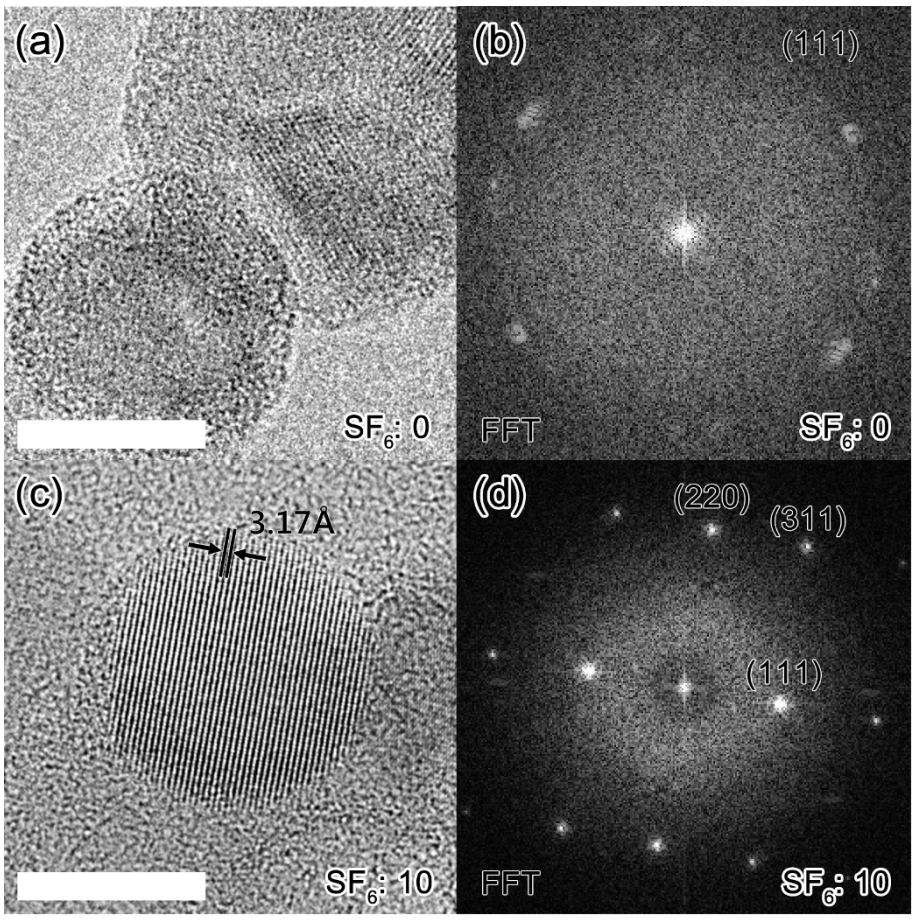

Fig. S8 TEM and its FFT images of Si-NPs produced without SF_6 gas (a and b) and with 10 sccm of SF_6 gas (c and d).

EDX TEM analysis of as-produced Si-NPs

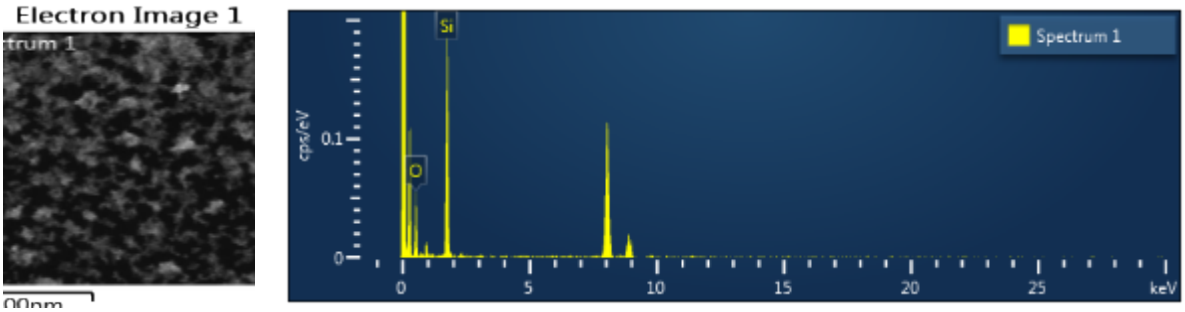

Element	Line Type	k factor	Absorption Correction	Wt%	Wt% Sigma	At%
O	K series	2.00744	1.00	30.21	2.57	43.10
Si	K series	1.00000	1.00	69.79	2.57	56.90
Total:				100.00		100.00

Fig. S9 EDX results under TEM of Si-NPs. Gas flow conditions are SiH_4 : 25, H_2 : 100, SF_6 : 0 sccm.

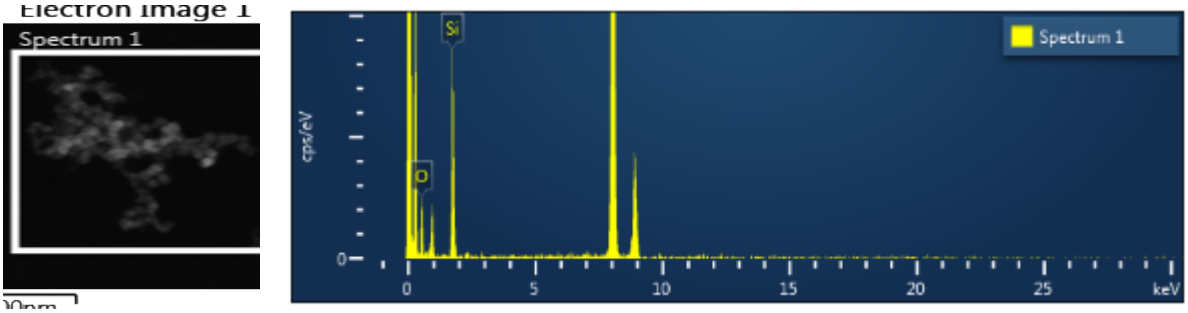

Element	Line Type	k factor	Absorption Correction	Wt%	Wt% Sigma	At%
O	K series	2.00744	1.00	33.05	3.21	46.35
Si	K series	1.00000	1.00	66.95	3.21	53.65
Total:				100.00		100.00

Fig. S10 EDX results under TEM of Si-NPs. Gas flow conditions are SiH_4 : 25, H_2 : 100, SF_6 : 10 sccm.

Table S2. Elemental analysis of Si-NPs by inductively coupled plasma atomic emission spectroscopy (ICP-AES)*

Si-NPs samples	Sulfur concentration (mg/kg)
Si-NP(-SF_6) (synthesis condition; SiH_4:25, H_2:100 sccm)	414 (0.04 %)
Si-NP(+SF_6) (synthesis condition; SiH_4:25, H_2:100, SF_6:10 sccm)	4,044 (0.4 %)

* The sulfur content in Si-NP(-SF_6) is thought to come from internal surface of the reactor contaminated by sulfur originating from previous runs for making Si-NP(+SF_6).

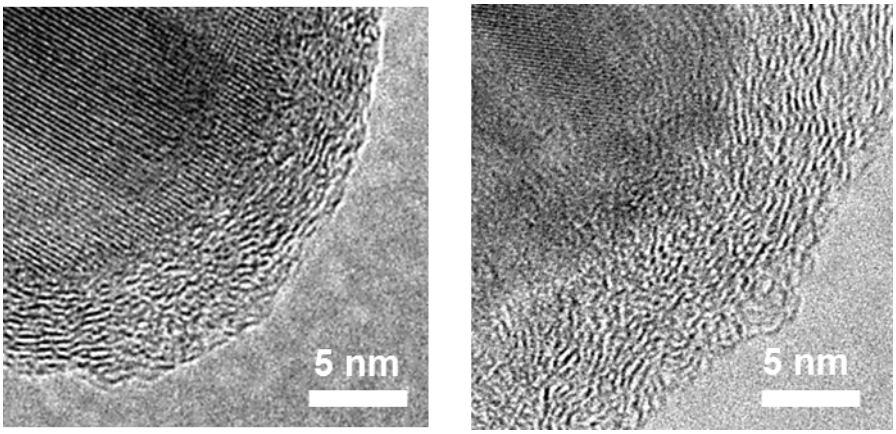

Fig. S11 TEM images of carbon-coated Si-NPs, left: Si-NP(+SF_6) and right: Si-NP(-SF_6)

Additional comments on Fig. 4.

One of the possible reasons for the capacity increase during the initial cycles (Fig. 4b) and after rate variation experiments (Fig. 4d) would be development of contacts between silicon and carbon black during cycles. At the first cycle, a portion of available mass of silicon is not lithiated due to the lack of the contacts and low conductivity of silicon. Electrodes experiencing repeated volume expansion and reduction of silicon during lithiation and delithiation generates more number of the contact points, utilizing additional mass of silicon that was not used in the previous cycle. After an initial period, capacities are saturated because all possible contacts are developed. This is supported by the increasing coulombic efficiency in the initial cycles. After the first cycle showing the smallest value of the coulombic efficiency, it takes up to 20 cycles for reaching reversible efficiency around 100 %. It means SEI layer formation still proceeds during the cycles because fresh surfaces of silicon that electrons can reach is developed.